# Design and Experimental Verification of Air Cooled Server Enclosure: A Novel Approach for Heat Sink Characterization

Ghazal Mohsenian<sup>1</sup>, Yaman Manaserh<sup>1</sup>, Mohammad Tradat<sup>1</sup>, Srikanth Rangarjan<sup>1</sup>, Ayushman Singh<sup>1</sup>, Koroush Nemati<sup>2</sup>, Alfonso Ortega<sup>3</sup>, and Bahgat Sammakia<sup>1</sup>

<sup>1</sup>Departments of Mechanical Engineering, ES2 Center, Binghamton University-SUNY, NY, USA

<sup>2</sup>Future Facilities, Inc., New York, NY, USA

<sup>3</sup>Villanova University, Villanova, PA, USA

E-mail: gmohsen1@binghamton.edu

Abstract — Semiconductor thermal management is becoming a bottleneck challenge that restricts further development in the electronics industry. Compromising processor requirements will impact the processor performance and reliability. Heat sinks are designed to increase the available surface area of an electronic component and allow for more heat to be easily dissipated. As a result, the thermal characterization of the heat sinks plays a critical role in electronics thermal management. In this study, a flexible experimental apparatus is designed, built, and assembled to characterize and test various electronics components in different aerodynamics and thermal conditions. This novel experimental apparatus allows for controlled characterization of the various heat sinks with different heights as well as realistic scenarios with air bypass at server level. Moreover, a general guideline on precise experimental procedure to characterize air cooled heat sinks is developed. The results show that introduced method reduces the experimental error by 26%.

Keywords— Component and Server Level Thermal Management, Air Cooling, Heat Sinks' Aerodynamic and Thermal Performance, Heat Sinks' Characterization

## I. INTRODUCTION

Data centers are one of the most energy-intensive building types, consuming 10 to 50 times the energy per floor space of a typical commercial office building [1]. There are many opportunities such as implementation of the containments systems, cooling control strategies development, electronics designs and measurements improvement to reduce energy use in data centers [2-18]. Due to advancements in processor technology, the thermal requirements for high performance CPUs are correspondingly rising. As a result, detailed thermal and hydraulic characterization and optimization of high performance heat sinks that are at the heart of most system level thermal management implementations is essential. Lei and Ortega [19-20] experimentally characterized hydraulic and thermal performance of the pin fin heat sinks under different top and side bypass conditions. A wind tunnel was fabricated from Plexiglass<sup>TM</sup>. The heat sink was installed at the center of the wind tunnel floor. Moreover, pressure taps were installed on one side of the wind tunnel for static pressure measurement. In another study, a suction-type wind tunnel was designed and built to test the hydraulic and thermal characteristics of the high

density-high aspect ratio heat sinks. A detailed static pressure and temperature measurements in fine pitch parallel plate copper heat sinks with and without top bypass flow was performed by Gutiérrez [21-22]. Duan et al. [23-24] developed a robust model for predicting pressure drop and thermal resistance of impingement air cooled plate fin heat sinks for different. To test the validity of the model, a flow bench was developed to measure the pressure drop of heat sinks with various impingement inlet widths, fin spacings, fin heights. Kumar et al. [25] experimentally investigated thermal and hydraulic performance of air cooled mini channel heat sinks with novel geometries including straight channel heatsink, wavy channel heatsink, and branch wavy channel. In another study, a comprehensive review of different Heat Sink (HS) designs, limiting factors, effectiveness, limitations of various techniques and recent advancements in the field of innovative heat sinks was conducted [26]. Klinkhamar et al. [27] characterized the heat transfer and pressure drop of the heat sink in terms of Reynolds number, Prandtl number, stand-off distance and jet-tojet spacing. Adhem et al. [28] looked into the methodologies used to analyze and optimize the overall performance of micro channel heat sinks. The literature assessment revealed that studies (from 1981 to 1999) were largely conducted using experimental or analytical methods while more recent studies (from 2000 to the end of 2012) were mostly done using numerical simulations and evolutionary algorithms. In this study, a novel experimental apparatus is designed and built to characterize the aerodynamic and thermal performance of aircooled heat sinks. What distinguished this work from previous studies is the flexibility of the experimental apparatus. The novel experimental setup provides the opportunity to test different heat sinks with various height, length and width. Moreover, the same flexible setup can be utilized to conduct component as well as server-level studies. Furthermore, precise and accurate experimental procedure for heat sinks characterization and measurements is introduced in this work.

#### II. DESIGN OF A FLEXIBLE EXPERIMENTAL APPARATUS

A flexible experimental apparatus is designed, built, and assembled to characterize and test various electronics

components in different aerodynamics and thermal conditions. One of the unique features of this setup is that the height, length, and width can be easily modified. Clear polycarbonate sheets are used for the top cover, side, and bottom walls to be able to observe the components, sensors and flow path inside the test chamber during the experiments. Multiple slots are drilled into the top cover sheet for a static pressure probe to be inserted and measured the pressure at different locations alongside the width and length of the server. The bottom plate consists of three sheets. The front and end sheets are made of clear polycarbonate and the middle sheet is made of ultra-high temperature Garolite sheet. A hole with a size of 1" ×1" is cut in the middle of the insulator sheet to be able to attach a heat source. Furthermore, two slots are drilled into the first and last bottom sheets which allow us to assemble the side walls using aluminum angles and change the width of the test chamber if required. The side walls' height can be adjusted and easily assembled to accommodate different server heights (1U, 2U, etc.). Moreover, another sheet is considered as a shelf at the bottom of the test apparatus. This setup has four wheels which enable ease of mobility. This apparatus can be used for component as well as server-level studies since all geometrical factors are adjustable. Figures 1 and 2 depict the detailed computer-aided design drawing of all the parts as well as the actual setup.

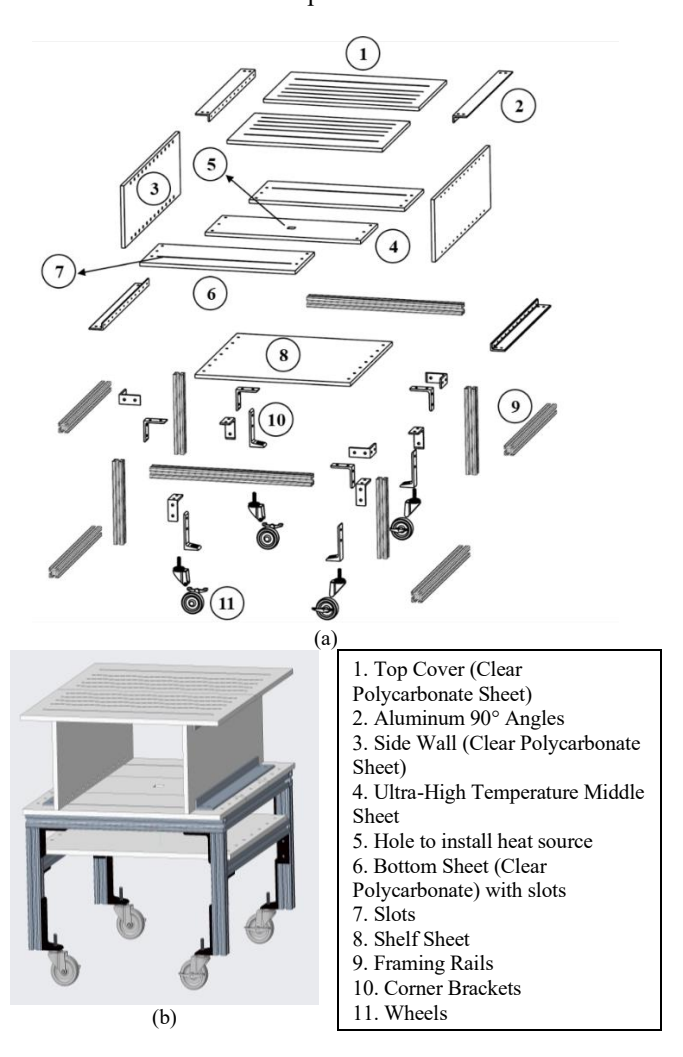


Fig. 1. (a) Detailed CAD drawing of different parts, (b) 3D-CAD drawing of the assembled experimental apparatus

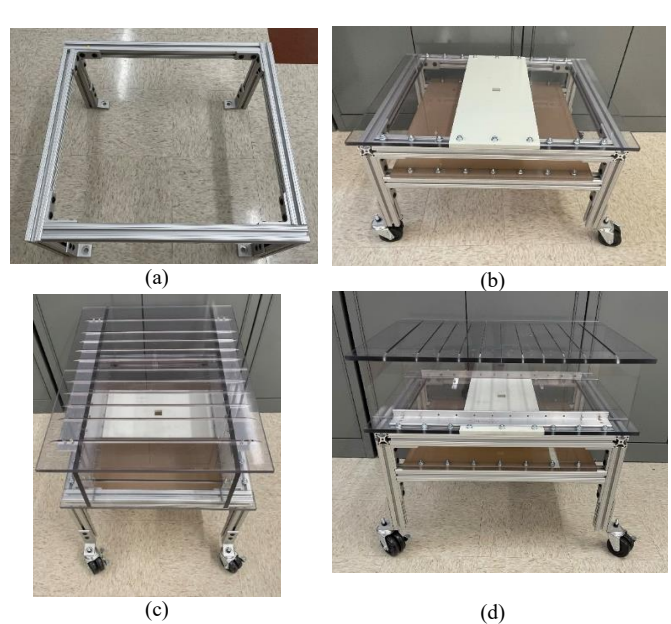


Fig. 2. Experimental apparatus, (a) Frame, (b) Bottom plate includes an insulator material with a hole in the middle, (c) Top view of the setup, (d)

Side view of the setup

# A. Heating Element

A  $1^{"}\times 1^{"}$  ceramic heater is used to mimic the die. The heater is constructed of aluminum nitride and it can provide up to 900 [W] power. The heater distributes the power uniformly which causes a uniform temperature contour taken by IR camera (Fig. 3b). Moreover, the ceramic heater has a K-type thermocouple with an accuracy of the  $\pm 0.75$  °C embedded inside. Ceramic insulation sheets are used to isolate the heater from the bottom and prevent any heat leakages as seen in Fig. 4. A high temperature and electrically insulating epoxy adhesive is used to attach the heater to the insulator material from the bottom.

In order to attach the heat sinks to the top of the ceramic heater, four holes are drilled into the insulator material (Fig. 5a). The heat sinks are attached to the Garolite with four springloaded fasteners placed at each corner of the base. The springloaded fastener applies 72 [PSI] of total pressure on the surface of the ceramic heater.

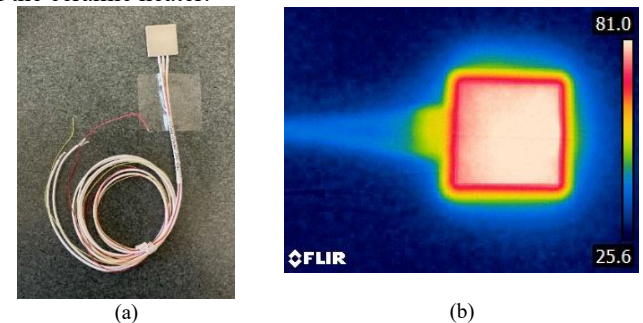


Fig. 3. Heating Element, (a) Ceramic heater, (b) IR camera temperature image

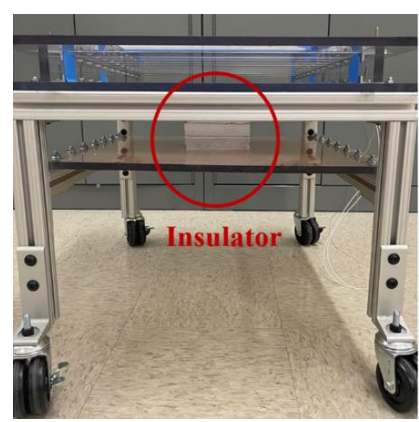


Fig. 4. Ceramic insulation sheets to prevent heat leakage from the bottom

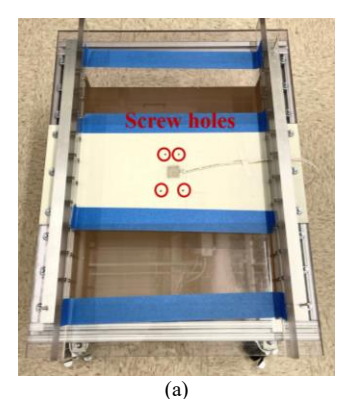




Fig. 5. (a) Four holes to attach HS on top of the heater, (b) 1U-HS is attached on top of the heater

#### B. Instrumentation

An airflow test chamber in accordance with AMCA 210-99/ASHRAE 51-1999 is used to measure impedance and thermal resistance curves of each heat sink. To cover the entire airflow range of the design, the chamber is constructed with a number of nozzles. The flow test chamber are built with pressure taps on each side of the nozzle to measure the differential pressure. The pressure taps near the end of the chamber is for measuring the differential pressure between the chamber and atmospheric pressure. The procedure of obtaining an impedance curve was explained by Alissa et al. [29]. The additional pressure readings are collected using static pressure probes with a diameter of 1.6 [mm] near each component (Fig. 6a). The pressure probe is connected to a MKS-120AD high accuracy pressure transducer using a tube. Two National Instruments (NI) Data Acquisitions (DAQs) namely c-DAQ-9171 and NI TB-9214 are used to gather the pressure and temperature readings. Moreover, a VARIAC (TDGC-2KM) variable transformer is used to regulate the supply voltage to the ceramic heater and consequently, change the heater power. In order to measure the inlet and outlet test chamber temperatures, three temperature/velocity mesh wooden frames are built as shown in Fig. 6e. The wooden frames dimensions are as follows:

- To cover a 1U test chamber:  $45 \times 7$  [cm<sup>2</sup>]
- To cover a 2U test chamber:  $45 \times 12$  [cm<sup>2</sup>]

# • To cover a 4U test chamber: $45 \times 18$ [cm<sup>2</sup>]

The Degree C velocity and temperature sensors are attached to the wooden frame, perpendicular to the airflow path. The Degree C velocity sensor accuracy is  $\pm 3\%$  of reading and thermistor accuracy is  $\pm 1$  [°C]. Furthermore, all of the temperature sensors and thermocouples are calibrated using PRECISION 605 high performance lab oven. The instrumentation and experimental setup are illustrated in Fig. 7.

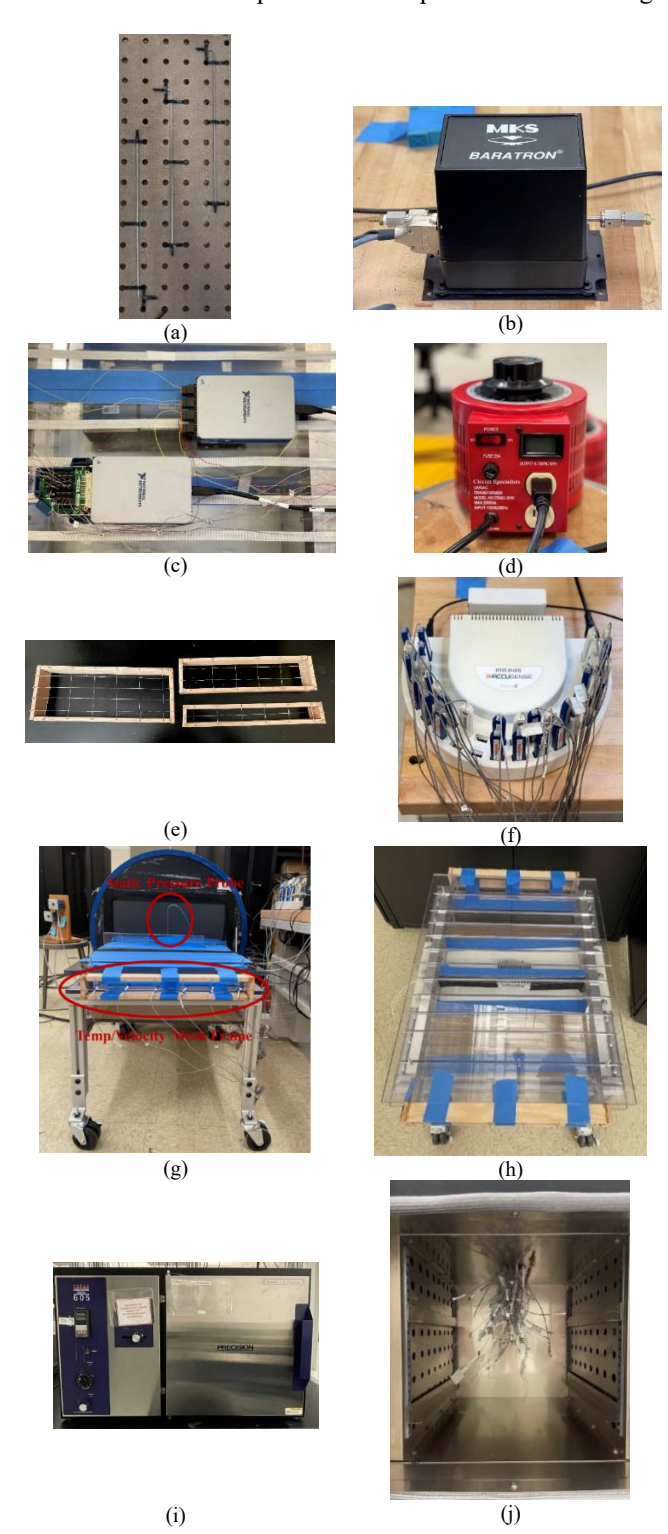


Fig. 6. Instrumentation, (a) Static pressure probes, (b) MKS pressure transducer, (c) NI-DAQs, (d) VARIAC voltage regulator, (e) Degree C sensors and DAQ, (f) Three temp/velocity mesh frames with different sizes, (g) Degree C sensors attached to the wooden frame, (h) Top view of a test chamber with wooden frames attached at the inlet and outlet, (i) PRECISION 605 high performance lab oven, (j) Sensors and thermocouples are inserted in the oven

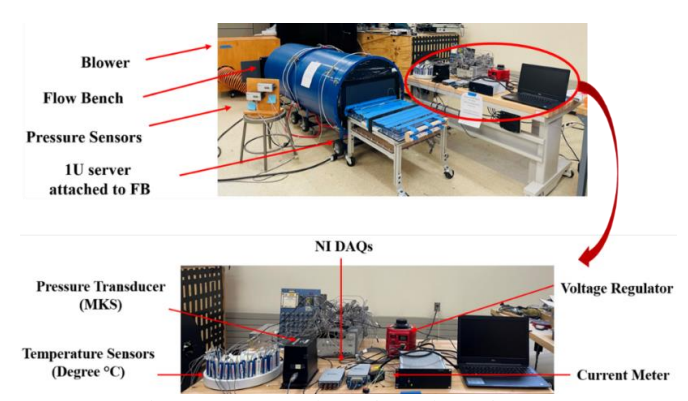


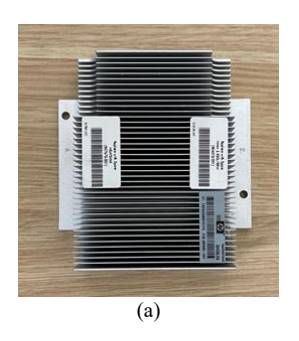
Fig. 7. Instrumentation and experimental setup

## III. HEAT SINKS

In this study, three different heat sinks are chosen to be characterized and compared to each other. Table 1 depicts the geometric characteristics of each HS in details. To characterize the heat sinks' thermal performance, three grooves are drilled into the base. Three T-type thermocouples with an accuracy of  $\pm 1$  [°C] are attached to the base of the heat sinks using thermally conductive adhesive in order to measure the base temperature. Figures 8-10 show the designs of three different heat sinks.

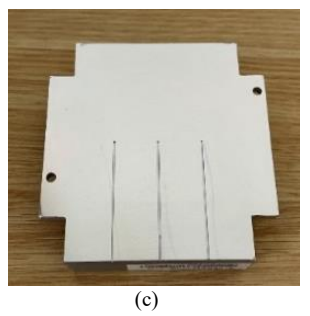
TABLE I. THREE DIFFERENT HEAT SINKS GEOMETRIC CHARACTERISTS

Heat Sinks	1U (HP-DL360 G6)	2U (Dell-R530)	4U (Dell-T430)
HS-Length	73 [mm]	105 [mm]	75 [mm]
HS-Width	98.6 [mm]	83 [mm]	85 [mm]
HS-Height	25 [mm]	40 [mm]	105 [mm]
Fin-Thickness	0.6 [mm]	0.34 [mm]	0.37 [mm]
Fin gap-Thickness	1.85 [mm]	2.2 [mm]	3.9 [mm]
Fin-Height	20 [mm]	35 [mm]	-
Base-Height	5 [mm]	5 [mm]	3.57 [mm]
Number of fins	41 [mm]	35 [mm]	20 [mm]





(b)



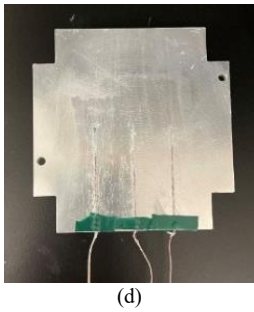
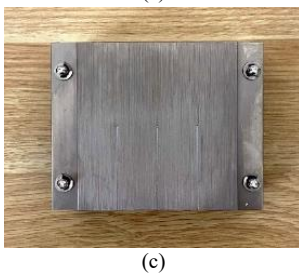


Fig. 8. 1U (HP-DL360 G6) heat sink, (a) Top view, (b) Side view, (c) Bottom view of the HS with three grooves drilled into the base, (d) Three thermoucouples are attached inside the grooves at the base of the HS







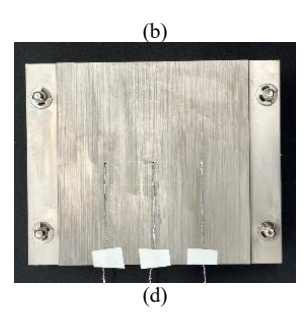
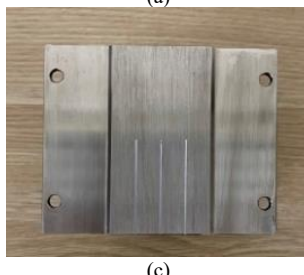


Fig. 9. 2U (Dell-R530) heat sink, (a) Top view, (b) Side view, (c) Bottom view of the HS with three grooves drilled into the base, (d) Three thermoucouples are attached inside the grooves at the base of the HS







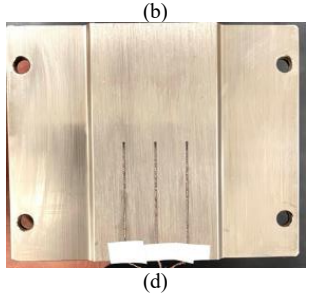


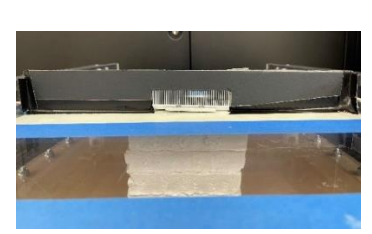
Fig. 10. 4U (Dell-T430) heat sink, (a) Top view, (b) Side view, (c) Bottom view of the HS with three grooves drilled into the base, (d) Three thermoucouples are attached inside the grooves at the base of the HS

#### IV. GUIDELINE FOR CHARACTERIZATION PROCEDURE

To characterize the aerodynamic and thermal behavior of the three heat sinks, they are installed in a confined test chamber without any side or top air bypass. At first, a 1U- HS is installed in a test chamber with the height of the 1U-HS= 25 [mm]. Afterward, two methods are proposed to confine the heat sinks surroundings. The first method is to install cardboard boxes to block any side air bypass around the HS. The experimental apparatus is shown in Fig. 11a.

The second method is to use the slots in the bottom sheets of the test apparatus and decrease the width of the chamber to match HS width (98.6 [mm]) as can be seen in Figures 11b and 11c.

To ensure accurate experimental procedure, a smoke test is done to observe the airflow path. A Mini Colt 4S smoke machine is used to generate smoke (Fig. 13a). As it is shown in Fig. 12a, using cardboard boxes to confine the heat sink's surrounding caused eddies and separation of the flow near the edges. Consequently, pressure drop across the HS increased for a constant flow rate by maximum of 26% (Fig. 12b). In conclusion, for precise aerodynamic and thermal characterization of the heat sinks, decreasing the width of the test apparatus using side walls to match the heat sinks width is suggested.







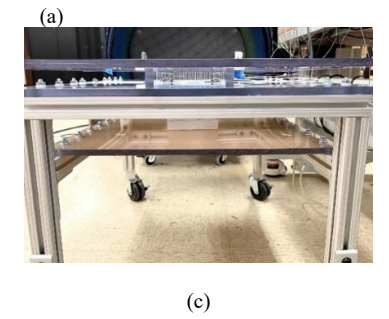
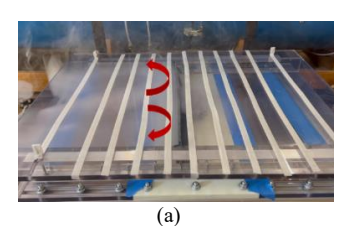


Fig. 11. Two different methods are introduced to confine the 1U-HS surrounding, (a) Using card board boxes around the HS, (b) Top view of the 1U-HS being confind using the side walls of the test apparatus, (c) Front view of the 1U-HS being confind using the side walls of the test apparatus



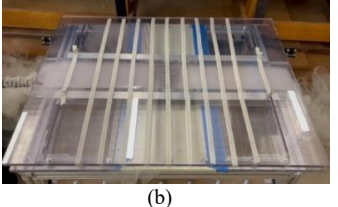


Fig. 12. Smoke Tests, (a) Using card board boxes around the HS, (b) Confining the HS using the test apparatus side walls

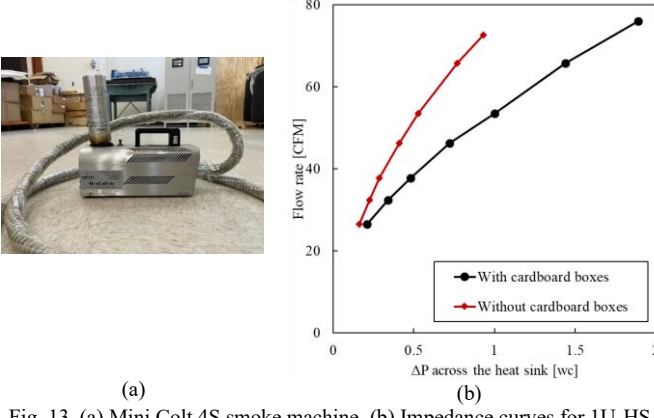


Fig. 13. (a) Mini Colt 4S smoke machine, (b) Impedance curves for 1U-HS using two different experimental methods

To acquire the heat sinks impedance curves, the blower flow rate is reported based on the differential pressure across the flow chamber nozzles. Simultaneously, the static pressure is measured inside the chamber near the inlet. Another technique is to insert a static pressure probe through the slots in the top cover and measure the static pressure near each component. The pressure measurements are taken in the direction of the flow. The distance between the heat sinks and static pressure probe is set to 7 [cm]. Figures 14b and 14c show the static pressure probes inserted from top cover to measure the pressure near the 2U and 4U heatsinks, respectively.

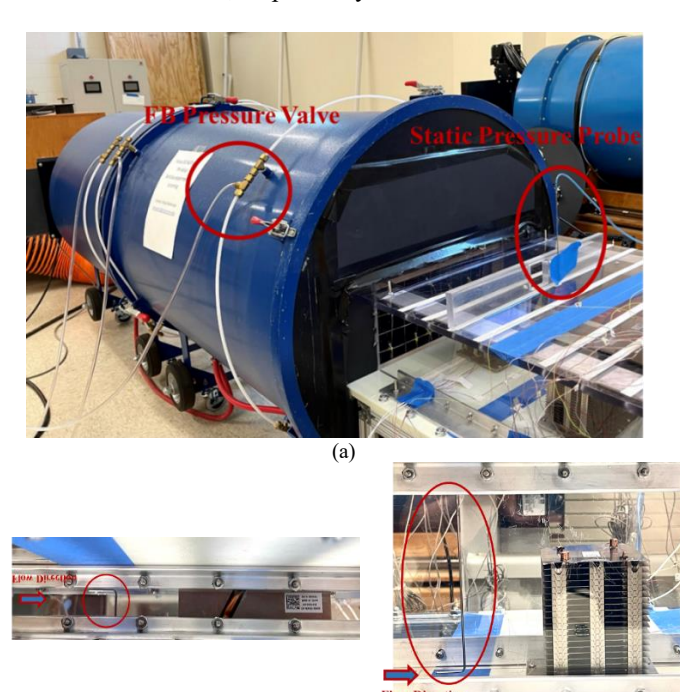


Fig. 14. (a) Pressure measurements location using flow bench pressure valve near the chamber inlet and static pressure probe near the components, (b) Static pressure probe inserted in a test chamber with the height of 2U-HS, (C) Static pressure probe inserted in a test chamber with the height of 4U

## V. EXPERIMENTAL VERIFICATION AND DISCUSSION

## A. Heat Sinks Aerodynamic Performance

To measure the impedance curves of the three heat sinks, the test chamber width and height are set to exactly match the HS under test dimensions (Figures 15b, 15d, and 15f). As can be seen in Fig. 15, the pressure measurements using flow bench pressure valve shows higher value compared to the static pressure probe for a constant flow rate. The reason is the longer distance and higher airflow resistance between HS and test chamber sensor. By increasing the flow rate, the pressure drop across the heat sinks rises. Fig. 16, depicts the impedance curves of the three heat sinks installed in a test chamber with their own size and without any air bypass. The performance of the 1U and 2U heat sinks are almost identical while the 4U-HS shows a higher aerodynamic performance compared to the others due to its larger height.

As a result, the aerodynamic performance of the three different heat sinks with various height is characterized using the same experimental apparatus.

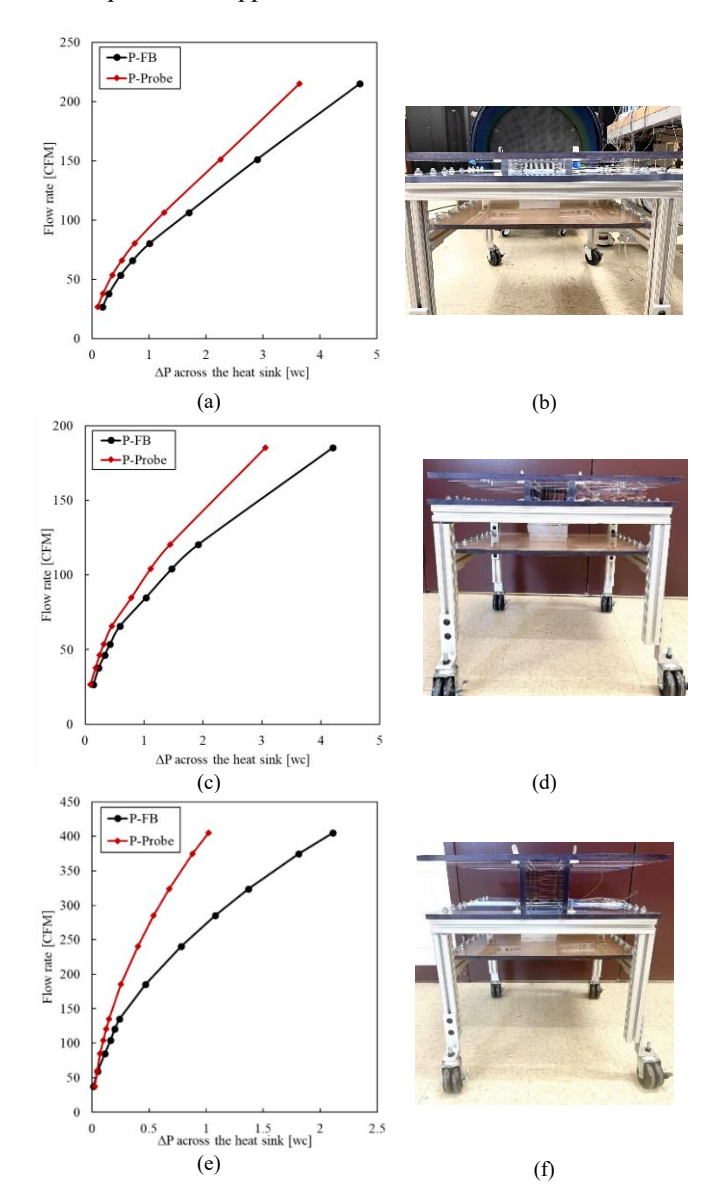


Fig. 15. Impedance curves using two different pressure measurement techniques, (a) Impedance curve for a 1U-HS without any air bypass, (b) The 1U-HS is installed in a 1U-HS test chamber, (c) Impedance curve for a 2U-HS without any air bypass, (d) The 2U-HS is installed in a 2U-HS test chamber, (e) Impedance curve for a 4U-HS without any air bypass, (f) The 4U-HS is installed in a 4U-HS test chamber

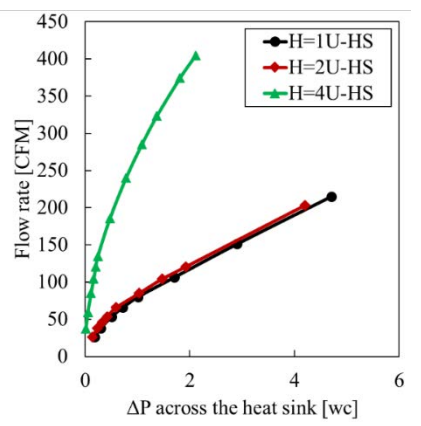


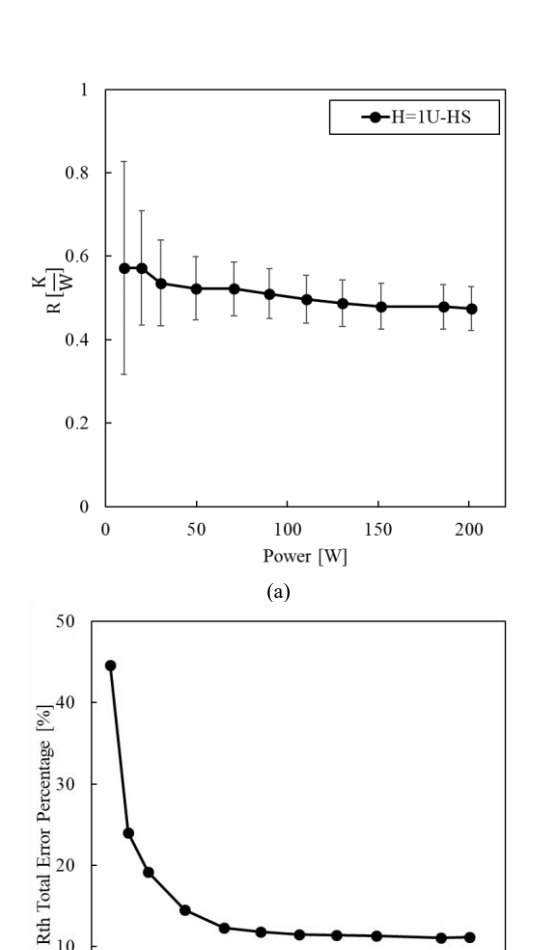
Fig. 16. Comparison between the three heat sinks impedance curves without any air bypass

#### B. Heat Sinks Thermal Performance

The thermal requirement of a HS is determined by calculating the junction-to-ambient thermal resistance. This is a basic thermal engineering parameter that can be used to evaluate and compare different thermal solutions. The thermal resistance of each heat sinks is calculated in a test chamber within the same size in terms of height and width. The heat sinks thermal resistance defined by equation (1).

$$R_{th=} \frac{T_{max}^{base} - T_{in}}{Q} \tag{1}$$

At first, the 1U-HS thermal performance is investigated. As shown in Fig. 17a, the rate of change in HS thermal resistance versus power is constant and equal to 0.49 . It should be noted that when variables represent experimental measurements, they have uncertainties due to measurement limitations which propagate due to the combination of variables in the function. The error propagation is higher for a lower power due to high percentage uncertainty in temperature at lower temperatures/power as shown in Fig. 17b. After q = 50 [W], the thermal resistance total error propagation decreases and measurements become reliable. Furthermore, the HS base temperature is measured using the attached three T-type thermocouples. The base temperature and heat flux have a linear relationship as shown in Fig. 17c. The cold air enters the HS, absorbs the most heat in the middle and finally exits from the opposite side. The middle thermocouple at the base of the HS is located at the center of the ceramic heater (Fig. 17d). As a result, the middle thermocouple measures higher temperature than front and back thermocouples. Furthermore, the back thermocouple measures higher temperature than the front thermocouple since the air temperature is increased after passing through the ceramic heater.



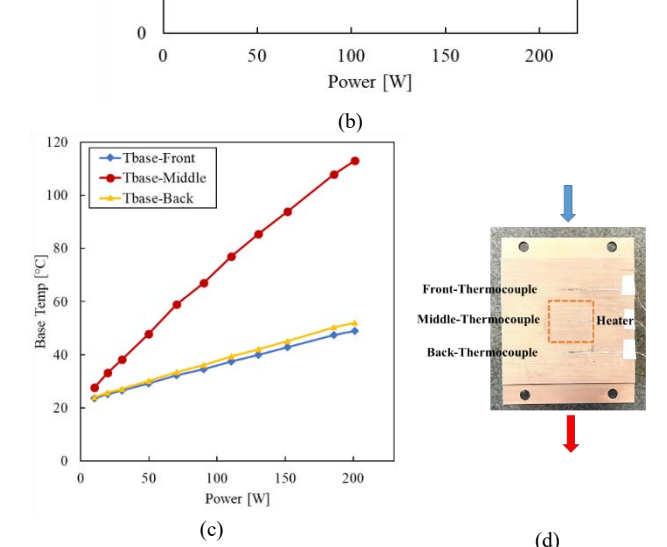


Fig. 17. (a) 1U-HS thermal resistance, (b) 1U-HS total error percentage, (c) 1U-HS base temperature vs. power, (d) The 1U-HS base schematic

It is important to understand and consider the impact of the interface between the ceramic heater and HS base on the overall thermal solution. Specifically, the bond line thickness, interface material area, and interface material thermal conductivity must be managed to optimize the thermal solution. It is critical to minimize the thickness of the TIM, commonly referred to bond line thickness. A large gap between the HS base and processor

case yields a greater thermal resistance. The total thermal resistance is calculated using equation (2) which has a higher value than the heat sink thermal resistance (equation (1)). As it is shown in Fig. 18a, the distance between the total and HS thermal resistance approximately stayed unchanged and equal to  $0.01 \left[\frac{K}{W}\right]$  which represents the summation of TIM and spreading thermal resistance.

The same procedure is repeated for 2U and 4U heat sinks. It is worth mentioning that the blower power is kept at 25 [W] throughout all of the experiments. As can be seen in Fig. 18b, the 4U-HS shows the lower thermal resistance than 1U and 2U heat sinks.

$$R_{\text{Tot}} = \frac{T_{\text{Heater}} - T_{\text{in}}}{q} \tag{2}$$

$$R_{\text{Tot}=} R_{\text{TIM+Spreading}} + R_{\text{HS}}$$
 (3)

$$R_{\text{TIM+Spreading}} = R_{\text{Tot}} - R_{\text{HS}} \tag{4}$$

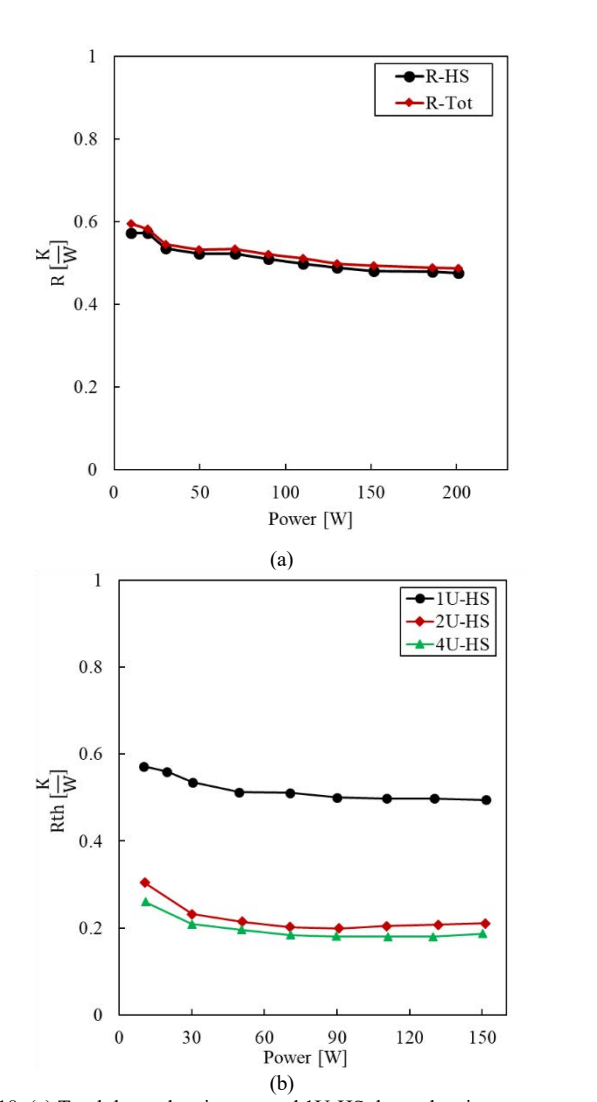


Fig. 18. (a) Total thermal resistance and 1U-HS thermal resistant vs. power, (b) Comparison between the three heat sinks thermal resistance curves without any air bypass

#### VI. CONCLUSIONS

A heat sink is a passive heat exchanger that used to maintain the die temperature within operating threshold. Any attempt to operate the server CPUs outside these limits may result in permanent damage to the die and potentially other components within the system. Maintaining the proper thermal environment is key to reliable and long-term system operation. In this study, a procedure of building a flexible experimental apparatus that can be used to test different heat sinks in different hydraulic and thermal conditions was discussed in detail. One of the unique features of this novel setup is that the height, length, and width of the setup can be easily modified. As a result, this apparatus can be used for component as well as server-level studies. That could help to mimic real time and controlled characterization scenarios. To prove the concept, the same setup is utilized to characterize three different heat sinks with various heights (1U, 2U, and 4U). Moreover, a general guideline on how to precisely characterize various air-cooled heat sinks was discussed.

The results show that using cardboard boxes to confine the heat sink's surrounding caused separation of the flow near the edges and increase the pressure drop across the HS. The novel test apparatus designed in this study has the capability to match the heat sink size which led to precise aerodynamic and thermal characterization of the heat sinks. The thermal resistance and differential pressure across the heat sinks is measured. The experimental results show that the 1U and 2U heat sink have almost the same impedance curves while more flow rate is required for a constant pressure using 4U-HS due to larger form factor. In addition, the heat sinks thermal resistance is independent of the power in single phase and 4U- HS has the best thermal performance compared to the 1U and 2U heat sink.

# REFERENCES

- [1] Department of Energy "Data Centers Energy Consumption." [online].

  Available https://www.energy.gov/eere/buildings/data-centers-and-servers. [Accessed: July 19th, 2022]
- [2] K. Nemati, H. A. Alissa, B. T. Murray, and B. Sammakia, "Steady-state and transient comparison of cold and hot aisle containment and chimney," in 2016 15th IEEE Intersociety Conference on Thermal and Thermomechanical Phenomena in Electronic Systems (ITherm), 2016, pp. 1435–1443. doi: 10.1109/ITHERM.2016.7517717.
- [3] R. Zhou, Z. Wang, C. E. Bash, and A. McReynolds, "Modeling and Control for Cooling Management of Data Centers With Hot Aisle Containment." pp. 739–746, Nov. 11, 2011. doi: 10.1115/IMECE2011-62506.
- [4] H. Rong, H. Zhang, S. Xiao, C. Li, and C. Hu, "Optimizing energy consumption for data centers," Renew. Sustain. Energy Rev., vol. 58, pp. 674–691, 2016.
- [5] W.-X. Chu and C.-C. Wang, "A review on airflow management in data centers," Appl. Energy, vol. 240, pp. 84–119, 2019.
- [6] S. K. Shrivastava and M. Ibrahim, "Benefit of Cold Aisle Containment During Cooling Failure," no. 55768. p. V002T09A021, 2013. [Online]. Available: http://dx.doi.org/10.1115/IPACK2013-73219
- [7] V. Sundaralingam, V. K. Arghode, Y. Joshi, and W. Phelps, "Experimental Characterization of Various Cold Aisle Containment Configurations for Data Centers," J. Electron. Packag., vol. 137, no. 1, pp. 11007–11008, Oct. 2014, [Online]. Available: http://dx.doi.org/10.1115/1.4028520
- [8] R. Khalid and A. P. Wemhoff, "Thermal Control Strategies for Reliable and Energy-Efficient Data Centers," J. Electron. Packag., vol. 141, no. 4, 2019

- [9] G. Mohsenian, S. Khalili, and B. Sammakia, "A Design Methodology for Controlling Local Airflow Delivery in Data Centers Using Air Dampers," in 2019 18th IEEE Intersociety Conference on Thermal and Thermomechanical Phenomena in Electronic Systems (ITherm), 2019, pp. 905–911.
- [10] G. Mohsenian et al., "A novel integrated fuzzy control system toward automated local airflow management in data centers," Control Eng. Pract., vol. 112, p. 104833, 2021, doi: https://doi.org/10.1016/j.conengprac.2021.104833.
- [11] G. Mohsenian, "A Novel Integrated Fuzzy Control System Towards Automated Local Airflow Management in Data Centers," State University of New York at Binghamton, Ann Arbor, 2020. [Online]. Available: http://proxy.binghamton.edu/login?url=https://www.proquest.com/disser tations-theses/novel-integrated-fuzzy-control-systemtowards/docview/2449439443/se-2?accountid=14168
- [12] T. D. Boucher, D. M. Auslander, C. E. Bash, C. C. Federspiel, and C. D. Patel, "Viability of Dynamic Cooling Control in a Data Center Environment," J. Electron. Packag., vol. 128, no. 2, pp. 137–144, Nov. 2005, [Online]. Available: http://dx.doi.org/10.1115/1.2165214
- [13] S. Khalili, "Airflow Management Using Active Air Dampers in Presence of a Dynamic Workload in Data Centers," SEMI-THERM 2019, 2019.
- [14] S.-W. Ham, M.-H. Kim, B.-N. Choi, and J.-W. Jeong, "Simplified server model to simulate data center cooling energy consumption," Energy Build., vol. 86, pp. 328–339, 2015, doi: https://doi.org/10.1016/j.enbuild.2014.10.058.
- [15] M. Tradat, G. Mohsenian, Y. Manaserh, B. Sammakia, D. Mendo, and H. A. Alissa, "Experimental Analysis of Different Measurement Techniques of Server-Rack Airflow Predictions Towards Proper DC Airflow Management," in 2020 19th IEEE Intersociety Conference on Thermal and Thermomechanical Phenomena in Electronic Systems (ITherm), 2020, pp. 366–373. doi: 10.1109/ITherm45881.2020.9190584.
- [16] K. Nemati, "Experimental and Computational Studies on the Role of Confinement Systems in Data Center Thermal Management," State University of New York at Binghamton, Ann Arbor, 2016. [Online]. Available: http://proxy.binghamton.edu/login?url=https://www.proquest.com/disser tations-theses/experimental-computational-studies-onrole/docview/1858569651/se-2?accountid=14168
- [17] S. Khalili et al., "Impact of Server Thermal Design on the Cooling Efficiency: Chassis Design," J. Electron. Packag., vol. 141, no. 3, Apr. 2019, doi: 10.1115/1.4042983.
- [18] G. Mohsenian et al., "A Novel Design of Rack Mount Server Thermal Simulator: Design, Assembly, and Experimental Verification," J. Electron. Packag., vol. 144, no. 4, Feb. 2022, doi: 10.1115/1.4053643.
- [19] N. Lei and A. Ortega, "Experimental hydraulic characterization of pin fin heat sinks with top and side bypass," in The Ninth Intersociety Conference on Thermal and Thermomechanical Phenomena In Electronic Systems (IEEE Cat. No.04CH37543), 2004, vol. 1, pp. 418-428 Vol.1. doi: 10.1109/ITHERM.2004.1319205.
- [20] N. Lei and A. Ortega, "Experimental Thermal Characterization of Pin Fin Heat Sinks With Top and Side Bypass," in International Electronic Packaging Technical Conference and Exhibition, 2005, vol. 42002, pp. 291–298.
- [21] F. E. O. Gutiérrez and A. Ortega, "Hydraulic and Thermal Characterization of Parallel Plate Fin Heat Sinks Under Side Inlet-Side Exit Flow Configuration, and Top Inlet-Side Exit Flow Configuration with and Without Top Flow Bypass," Univ. Arizona, Arizona, USA, 2005.
- [22] F. E. Ortega Gutierrez, A. Ortega, and G. Xu, "Experiments on the Flow and Heat Transfer in Fine Pitch Parallel Plate Heat Sinks With Side Inlet Side Exit Flow," in International Electronic Packaging Technical Conference and Exhibition, 2005, vol. 42002, pp. 315–327.
- [23] Z. Duan and Y. S. Muzychka, "Impingement air cooled plate fin heat sinks. Part I - Pressure drop model," in The Ninth Intersociety Conference on Thermal and Thermomechanical Phenomena In Electronic Systems (IEEE Cat. No.04CH37543), 2004, vol. 1, pp. 429-435 Vol.1. doi: 10.1109/ITHERM.2004.1319206.

- [24] Z. Duan and Y. S. Mzychka, "Impingement air cooled plate fin heat sinks. Part II - Thermal resistance model," in The Ninth Intersociety Conference on Thermal and Thermomechanical Phenomena In Electronic Systems (IEEE Cat. No.04CH37543), 2004, vol. 1, pp. 436-443 Vol.1. doi: 10.1109/ITHERM.2004.1319207.
- [25] S. Kumar, M. Sarkar, P. K. Singh, and P. S. Lee, "Study of thermal and hydraulic performance of air cooled minichannel heatsink with novel geometries," Int. Commun. Heat Mass Transf., vol. 103, pp. 31–42, 2019.
- [26] Z. Khattak and H. M. Ali, "Air cooled heat sink geometries subjected to forced flow: A critical review," Int. J. Heat Mass Transf., vol. 130, pp. 141–161, 2019.
- [27] C. Klinkhamer, S. Abishek, K. L. V Iyer, R. Balachandar, and R. Barron, "Characterization of a Jet Impingement Heat Sink for Power Electronics Cooling," Therm. Sci. Eng. Prog., p. 101408, 2022, doi: https://doi.org/10.1016/j.tsep.2022.101408.
- [28] A. Mohammed Adham, N. Mohd-Ghazali, and R. Ahmad, "Thermal and hydrodynamic analysis of microchannel heat sinks: A review," Renew. Sustain. Energy Rev., vol. 21, pp. 614–622, 2013, doi: https://doi.org/10.1016/j.rser.2013.01.022.
- [29] H. A. Alissa, K. Nemati, B. G. Sammakia, K. Schneebeli, R. R. Schmidt, and M. J. Seymour, "Chip to Facility Ramifications of Containment Solution on IT Airflow and Uptime," IEEE Trans. Components, Packag. Manuf. Technol., vol. 6, no. 1, pp. 67–78, 2016, doi: 10.1109/TCPMT.2015.2508453.G. Eason, B. Noble, and I. N. Sneddon, "On certain integrals of Lipschitz-Hankel type involving products of Bessel functions," Phil. Trans. Roy. Soc. London, vol. A247, pp. 529–551, April 1955. (references)